

Solid-state time-gated luminescence microscope with ultraviolet light-emitting diode excitation and electron-multiplying charge-coupled device detection

Russell Connally

James Piper

Macquarie University
Centre for Laser Applications
Sydney, Australia 2109

Abstract. Many naturally occurring materials are autofluorescent, a property that can reduce the discriminative ability of fluorescence methods, sometimes to the point where they cannot be usefully applied. Shifting from the spectral to the temporal domain, it is possible to discriminate fluorophores on the basis of their fluorescence decay lifetime. Luminophores with sufficiently long lifetimes can be discriminated from short-lived autofluorescence using time-gated luminescence (TGL). This technique relies upon the application of a brief excitation pulse followed by a resolving period to permit short-lived autofluorescence to decay, after which detection is enabled to capture persistent emission. In our studies, a high-power UV LED was mounted in the filter capsule of an Olympus BX51 microscope to serve as the excitation source. The microscope was fitted with an Andor DV885 electron-multiplying CCD (EM-CCD) camera with the trigger input synchronized to UV LED operation. *Giardia lamblia* cysts labeled with the europium chelate BHHST were analyzed against an autofluorescent background with the TGL microscope. The EM-CCD camera captured useful TGL images in real time with a single exposure cycle. With 4x frame averaging, images acquired in TGL mode showed a 30-fold improvement in SNR compared with conventional fluorescence microscopy. © 2008 Society of Photo-Optical Instrumentation Engineers. [DOI: 10.1117/1.2928169]

Keywords: time-gated luminescence; UV LED; europium; chelate; lanthanides; *Giardia lamblia*; autofluorescence.

Paper 07472R received Nov. 25, 2007; revised manuscript received Jan. 15, 2008; accepted for publication Jan. 15, 2008.

1 Introduction

Many naturally occurring substances are autofluorescent when excited with UV or visible wavelengths. Autofluorescence emission typically spans the visible spectrum with a lifetime (τ) measured in nanoseconds. One of the earliest reports of using a probe fluorescence lifetime (τ) to discriminate against nonspecific background autofluorescence was made by Thayer and Sernetz in 1973.¹ Since then, a number of microscopes with the ability to resolve different fluorophores on the basis of τ have been reported.²⁻⁵ Instruments that operate in the time domain to resolve fluorophores that differ in τ by a large degree (ns versus μ s) have the advantage of simplicity and lower cost compared to microscopes required to resolve fluorophores on the basis of a few nanoseconds' difference. The time-gated luminescence (TGL) microscope described here operates within the time domain to capture long-lived (greater than 100 μ s) emission after autofluorescence has decayed. Figure 1 illustrates the basic concept of TGL; with the detector off, the TGL cycle begins with a short, powerful excitation

pulse that raises the target luminophore into its excited state. On termination of the excitation pulse, nonspecific fluorescence decays rapidly while target luminescence persists for orders of magnitude longer. After a resolving period (gate delay), the detector is gated on (acquisition period) to capture luminescent emission in the absence of autofluorescence.

TGL microscopes employ a pulsed excitation scheme at a wavelength suited to the target luminophore. Platinum and palladium porphyrin based luminophores can be excited at either 390 or 540 nm; a number of solid-state or semiconductor excitation sources are suitable for this role. Unlike the former compounds, lanthanide chelates are not oxygen sensitive and can provide longer lifetimes (0.5 to 2 ms). They are normally employed with the ions bound to a sensitizer molecule to boost the absorbance cross-section. Typically they require excitation in the UV region of the spectrum (Tb³⁺: 320 nm; Eu³⁺: 337 nm), with the upper useful limit being about 370 nm for terpyridine-based europium chelates (~15% effective at 337 nm). Some europium chelates in novel configurations can be excited at longer wavelengths (365 to 400 nm), although they were not used for this work due to other important limitations.⁶⁻⁹ The luminescence life-

Address all correspondence to Russell Connally, Physics Department, Division of Information & Communication Sciences, Macquarie University, Balaclava Road, Sydney, NSW 2109 Australia; Tel: +61 2 9850 8111; Fax: +61 2 9850 8115; E-mail: rconnall@ics.mq.edu.au

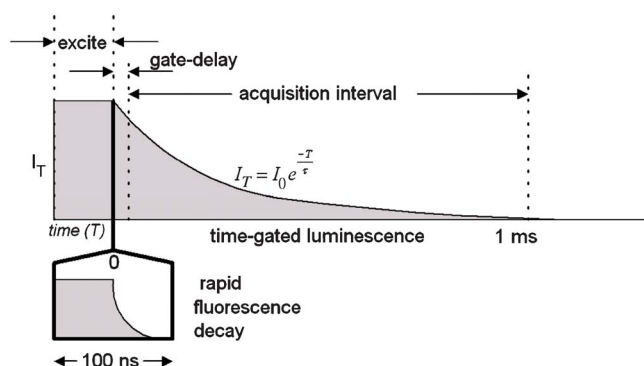


Fig. 1 TGL suppresses autofluorescence by delaying signal acquisition until prompt (auto-fluorescence) has faded. Lanthanide chelate luminescence can persist for milliseconds, greatly facilitating its detection in the absence of autofluorescence.

44 time of europium chelates is typically around 300 to 600 μ s
 45 in aqueous environments and follows single exponential de-
 46 cay kinetics.

47 Microscopes designed for use with lanthanide chelates
 48 usually employ pulsed UV sources such as Xe flashlamps, or
 49 nitrogen-laser or chopper-interrupted Hg arc lamps.¹⁰⁻¹⁵ As a
 50 consequence of their low duty cycle, phosphors emit rela-
 51 tively weakly compared with most fluorophores and therefore
 52 require sensitive detectors. All previously reported TGL mi-
 53 crosopes have required multiple excitation detection cycles
 54 to deliver an image of acceptable contrast and quality. The
 55 detector integrates photons over many TGL cycles, and it is
 56 necessary to shield the sensor from light during the excitation
 57 cycle. Microchannel-plate image intensifiers that employ elec-
 58 tronic gating are used to satisfy this requirement, whereas
 59 conventional CCD cameras require an external shutter mecha-
 60 nism. Regardless of the technique used, multiple excitation
 61 cycles have been necessary, requiring either an expensive
 62 gated image intensifier,^{11,14-21} a vibration-prone mechanical
 63 beam interrupter (chopper),^{12,22} or a high-insertion-loss ferro-
 64 electric LCD shutter^{14,20} to control the light reaching the de-
 65 tector.

66 We previously reported the design of a UV LED-excited
 67 TGL microscope for use with europium fluorophores.²³ The
 68 recent availability of electron-multiplying CCD (EM-CCD)
 69 cameras prompted us to consider their application in TGL
 70 microscopy. EM-CCD cameras are the solid-state equivalent
 71 of image-intensified CCD cameras, albeit with lower gain,
 72 which is compensated to some extent by a threefold improve-
 73 ment in quantum sensitivity.

74 While EM-CCD cameras offer high sensitivity, they still
 75 require an external shutter mechanism if multiple TGL cycles
 76 are to be employed for each acquisition. Alternatively, if a
 77 single exposure cycle is sufficient, as with the system de-
 78 scribed here, the shutter can be eliminated.

79 2 Method

80 2.1 UV LED

81 Due to the small size of the LED, the device was mounted
 82 within an Olympus U-MWU2 filter cube as shown in Fig. 2.
 83 The UV LED (NCSU033A, Nichia Corp., Japan) used for this

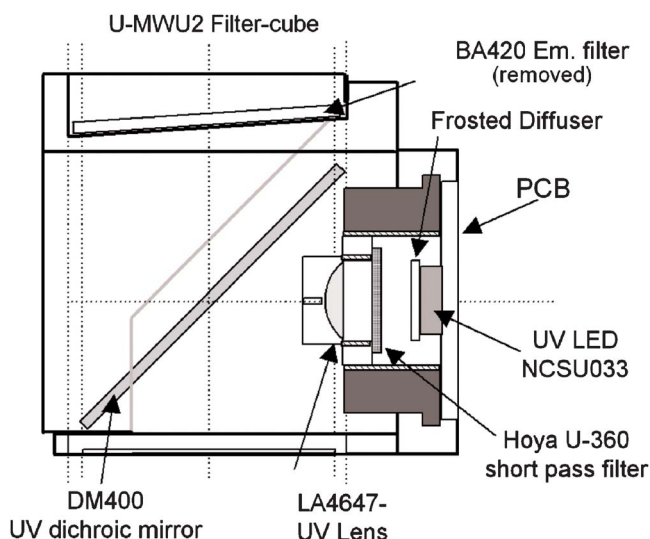


Fig. 2 Cutaway view of the U-MWU2 Olympus filter cube illustrating the optical components of the Nichia NCSU033 UV LED excitation scheme. Due to the narrow passband of the LED emission, both the excitation and emission filters were removed from the filter assembly for this work.

work was an improved device rated at 220 mW (365 nm) at 84
 500 mA, about double the output power of the previous ver- 85
 sion (NCCU033). The LED was surface-mounted to a 25- 86
 mm-diameter single-sided PCB that replaced the excitation 87
 filter in the cube. In the confined space of the cube, it was not 88
 possible to achieve Koehler illumination and a diffuser 89
 (frosted glass slide) was mounted on the front face of the LED 90
 to homogenize the beam. To the eye, the excitation region 91
 appeared uniform in intensity, although scatter from the dif- 92
 fuser was estimated to reduce output power by about 15%. 93
 Power was supplied to the LED via flexible power leads that 94
 entered the filter housing at its central axis to permit filter 95
 cubes on either side of the UV LED to be rotated into view. 96
 The filter housing was thus limited to rotation ± 60 deg from 97
 the UV LED axis due to the length of the power leads. 98

Earlier we reported the existence of low-intensity self- 99
 excited visible luminescence from InGaN-based LEDs that 100
 persists for some time following switch-off and that can 101
 present a problem when the devices are used in pulse fluo- 102
 rometry applications.^{24,25} To suppress this component, a short- 103
 pass filter (Hoya U-360, Edmund Optics, Singapore) was in- 104
 cluded in the excitation beam path that was situated about 105
 3 mm from the LED face, as shown in Fig. 2. A fused silica 106
 lens $\phi=12.7$ mm, $f.l=20$ mm (LA4647-UV, Thorlabs, New- 107
 ton, New Jersey) was mounted approximately 16 mm from 108
 the LED face to collimate the excitation radiation. The filtered 109
 excitation beam was then directed into the microscope objec- 110
 tive via the DM400 dichroic mirror. This mirror strongly re- 111
 flects wavelengths below 380 nm while transmitting visible 112
 (>400 nm) light better than 90%. The increased optical clar- 113
 ity of this arrangement helped maximize fluorescence and ex- 114
 citation efficiency of the instrument. 115

2.2 Instrumentation 116

An Olympus BX51 fluorescence microscope was used for this 117
 work, and images were acquired without the benefit of spec- 118

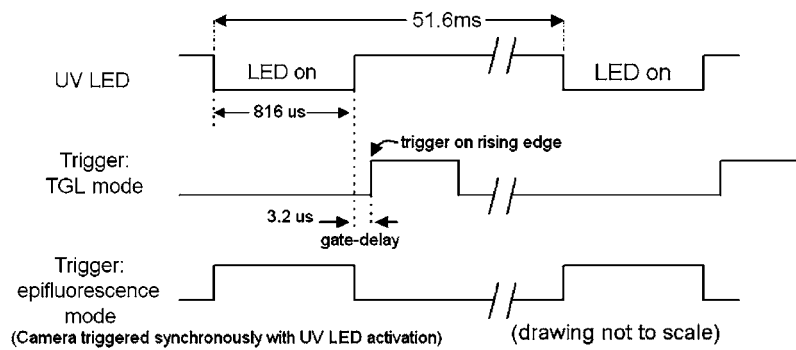


Fig. 3 Pulse timing for the UV LED and camera trigger pulse when operated in conventional epifluorescence mode (prompt). While this mode of operation uses a pulsed source, it appears continuous to the camera and eye, returning conventional fluorescence images. Rise time of the LED pulse on turn-off was $1.33 \text{ V}/\mu\text{s}$; the camera was triggered about $3.2 \mu\text{s}$ after the LED pulse. This small gate-delay resulted in a loss of about 1% of the initial intensity of the europium label at the moment of acquisition.

119 tral filtering. The UV-LED was supplied from a program-
 120 mable voltage source so that it could be driven at two differ-
 121 ent power levels. The LED current was monitored by
 122 measuring the peak voltage across the 5-ohm LED load resis-
 123 tor with an oscilloscope; in low-power mode, the current was
 124 288 mA at a supply voltage of 5.5 V, and in high-power
 125 mode, it was 1.44 amps at 11.6 V. The LED was always
 126 operated in pulsed mode, and it was convenient to switch to
 127 low-power mode to limit photobleaching when higher-duty
 128 cycles or long observation periods were employed.

129 2.3 LED Output Power

130 A Coherent FieldMax™ -TO laser power meter fitted with a
 131 model PS10Q detector head was used for power measure-
 132 ments. The output face of the U-MWU2 filter cube was fixed
 133 approximately 2 cm from the PS10Q sensor for power mea-
 134 surements. The pulse profile for both the TGL and epifluores-
 135 cence modes is shown in Fig. 3. The rising edge of the trigger
 136 pulse would shift from the start to the end of the UV LED
 137 pulse when it was switched from prompt (epifluorescence)
 138 mode to TGL mode. The duration of the LED pulse was
 139 $816 \mu\text{s}$ with a 51.6-ms resting period between each pulse,
 140 corresponding to a frequency of 19.38 Hz and a duty cycle of
 141 1:63. The observed average power was $370 \mu\text{W}$ with a cal-
 142 culated peak power of 23.4 mW. In idle mode (volts
 143 = 5.5 V), the observed average power was $105 \mu\text{W}$ with a
 144 calculated peak power of 6.64 mW. The LED (still fitted with
 145 the diffuser) was then removed from the filter cube and placed
 146 2 cm from the sensor. In TGL mode, the average power read-
 147 ing was 1.205 mW with a peak power of 76.2 mW, or 3.05-
 148 fold higher than when mounted in the cube. In idle mode, the
 149 average power was $275 \mu\text{W}$ with a 17.4-mW peak power,
 150 corresponding to 2.6 times the power level when mounted in
 151 the cube.

152 By comparison, our previously reported UV-LED filter as-
 153 sembly, which lacked both the diffuser and the Hoya 360
 154 filter, delivered an average power of $470 \mu\text{W}$ with a
 155 29.72-mW peak (LED in filter cube) when measured with the
 156 FieldMax™ power meter.²³

2.4 EM-CCD Camera

157
 158 An iXon DV885 EM-CCD was fitted to the microscope using
 159 a standard C-mount lens adaptor. The DV885 camera specifi-
 160 cations include: Texas Instruments 1004 \times 1002 Impactron
 161 frame transfer CCD sensor, $8 \times 8 \mu\text{m}$ pixels, EM gain 2000,
 162 quantum efficiency of 65% at 600 nm, 14-bit digitized output,
 163 24 full frames per second, and external trigger mode support.
 164 An embedded microcontroller was used to control the camera,
 165 which was operated in “fast external trigger” mode so the
 166 instrument could be switched instantly between conventional
 167 “prompt” fluorescence and TGL modes. To make the system
 168 more versatile, a microcontroller was used to control the gate-
 169 delay interval, repetition frequency, trigger pulse polarity,
 170 LED pulse length, and drive intensity parameters. In fast-
 171 trigger mode the sensor and its registers are cleared pending
 172 the arrival of the trigger pulse, the rising edge of which initi-
 173 ates frame capture within nanoseconds. A gate delay of
 174 $3.2 \mu\text{s}$ was imposed between the termination of the LED
 175 pulse and the rising edge of the trigger pulse.

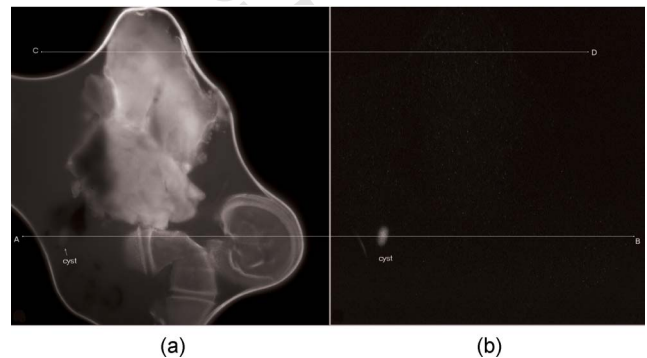


Fig. 4 Line A-B transects a BHHST-labeled *Giardia* cyst that was (a) captured in conventional epifluorescence mode and (b) acquired in TGL mode. The cyst in this instance was encountered within an island of fluid containing the fluorescent dye DMACA together with autofluorescent debris from the water concentrate. A bright region of autofluorescence was sampled along the second line profile C-D and compared with the same region captured in TGL mode.

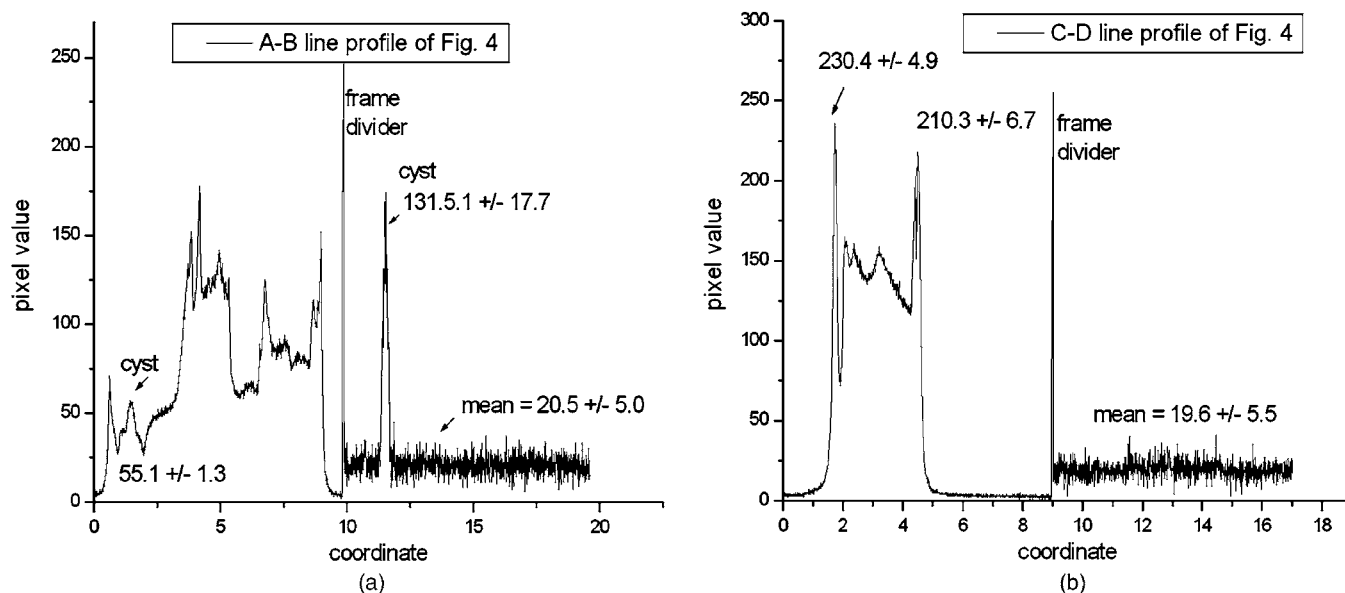


Fig. 5 (a) Line profile A-B was sampled to compare pixel values on the labeled cyst for prompt and TGL modes. (b) Second line profile C-D in Fig. 4 transits a strongly fluorescent region that was used to determine the effectiveness of TGL suppression. Data from both regions was used to calculate the improvement in SNR (30-fold).

176 2.5 Test Sample

177 *Giardia lamblia* cysts (Biotech Frontiers Pty. Ltd., Sydney,
 178 Australia) were labeled using the europium chelate BHHST
 179 (4,4'-bis-(1'',1'',1'',2'',2'',3'',3''-heptafluoro-4'',6''-hexane-
 180 dion-6''-yl) sulfonyl-aminopropyl-ester-N-succinimide-ester-
 181 *o*-terphenyl), the synthesis and use of which has previously
 182 been reported.²⁶ The 10,000:1 concentrate isolated from the
 183 Sydney water supply used for this work was a kind gift from
 184 Dr. Belinda Ferrari and was prepared from 10 L backwash
 185 water samples using the flocculation method.²⁷ To further in-
 186 crease the autofluorescence background, the UV excitable
 187 fluorophore 7-dimethylaminocoumarin-4-acetic acid
 188 (DMACA) was added to the water concentrate together with
 189 the *Giardia* cysts.

190 3 Results and Discussion

191 The addition of DMACA resulted in strong background fluo-
 192 rescence that limited visibility of the *Giardia* cyst situated at
 193 the bottom-left of Fig. 4(a). This 8-bit image was acquired
 194 using a 40X objective, a 3-ms exposure with averaging en-
 195 abled (4 x frames), and EM gain turned off. Figure 4(b) was

acquired after the microscope was switched to TGL mode and 196
 EM gain was increased to 1185. The line A-B transects the 197
 cyst in both the prompt and TGL capture frames to generate 198
 the profile shown in Fig. 5(a). For background determination, 199
 the second line profile C-D was sampled; pixel values for this 200
 trajectory are shown in Fig. 5(b). Data points from these two 201
 sets were analyzed to determine the effective improvement in 202
 the signal-to-noise ratio (SNR), and key values used for this 203
 calculation are shown in Table 1. The SNR figures were based 204
 on the average 8-bit intensity value of the cyst referenced to 205
 the brightest region of nonspecific fluorescence within the 206
 frame. In prompt epifluorescence mode, the cyst emitted 207
 weakly in comparison with other regions and a SNR of 208
 0.23 ± 0.012 was obtained. In TGL mode, the cyst was the 209
 only object visible and the SNR improved 30-fold to a value 210
 of 7.04 ± 2.58 . The relatively large error bars arise from the 211
 small sample size of 17 (for the cyst) with pixel values rang- 212
 ing from 104 to 174. 213

3.1 Effect of Frame Averaging 214

Software supplied with the iXon camera provided the option 215
 to average successive frames and improve image quality 216

Table 1 Summary of the input values used to calculate the improvement in SNR for the *Giardia* cyst shown in Fig. 4. To compare Figs. 4(a) and 4(b), the SNR was determined by sampling identical regions and calculating the ratio of the brightest signal to the brightest (autofluorescent) background. The effective improvement was taken as the ratio of TGL_{SNR} to $PROMPT_{SNR}$.

Mode	Prompt				TGL			
	Average	SD	<i>n</i>	SNR	Average	SD	<i>n</i>	SNR
Cyst	54.5	1.74	9	0.23 ± 0.012	131.5	17.7	17	7.04 ± 2.58
Background	230.4	4.9	5		20.5	5.0	601	

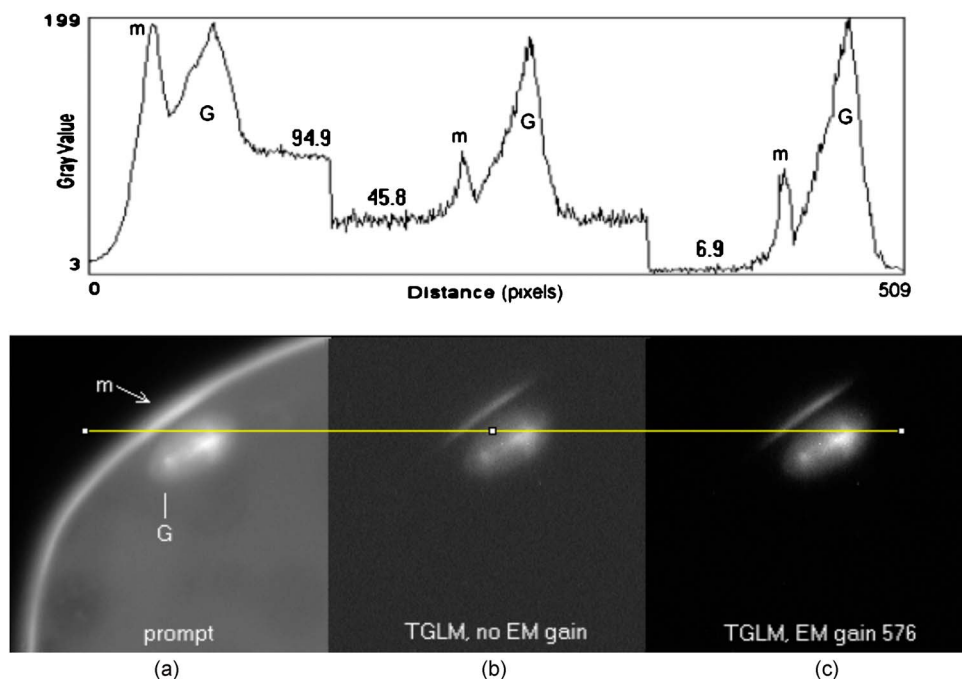


Fig. 6 A BHHST-labeled *Giardia* cyst (labeled G) suspended in an aqueous solution of DMACA was captured in (a) conventional epifluorescence mode, (b) TGL mode without the assistance of EM-gain, and (c) TGL mode with EM-gain enabled. The line profile shown above the sequence illustrates graphically the reduction in background that was achieved in each of these modes. SNR was improved progressively from 1 to 4.6 to 28 in Fig. 6(c). The arc-shaped region to the left of the cyst in Figs. 6(b) and 6(c) arises from cyst luminescence reflected by the liquid meniscus (m) as the DMACA solution evaporated.

217 through reduction of random noise components. Averaging
218 significantly improved the SNR by decreasing the background
219 noise level. For example, a background region (sample
220 count=15,104 pixels) within a single frame acquired under
221 TGL conditions had an average value of 21.58 ± 4.78 . When
222 the same frame was averaged over four successive frames, the
223 background dropped to 12.97 ± 2.59 . Increasing the frame
224 count to 8 resulted in a further small improvement in SNR
225 (about 7%).

226 The improvement in signal strength achieved by frame av-
227 eraging was determined by monitoring an oval region (sample
228 count=532 pixels) on a *Giardia* cyst present within the
229 frames captured for background measurements. The mean
230 pixel value for the region after a single acquisition was
231 163.1 ± 28.96 , and this was improved to 177.7 ± 28.91 when
232 four successive frames were averaged (data not shown).

233 3.2 EM Gain and its Effect on SNR

234 BHHST is a strongly luminescent europium chelate that was
235 conjugated to the anti-*Giardia* monoclonal antibody G203 for
236 the detection of *Giardia lamblia* cysts. The iXon camera em-
237 ploys a very sensitive sensor, and it was possible to capture
238 images of well-labeled *Giardia* cysts even without the assis-
239 tance of EM gain. Figure 6(a) was captured in conventional
240 epifluorescent mode and shows an image of a *Giardia* cyst
241 suspended within a background of fluorescent DMACA. The
242 line profile at the top reports pixel intensity from left to right
243 across the three frames [6(a) to 6(c)], and the fluid meniscus
244 and center of the cyst have roughly equal (peak) pixel inten-
245 sities. Figure 6(b) was captured in TGL mode with EM gain
246 turned off. Referring again to the line profile, it is apparent

that fluorescence from the DMACA was strongly suppressed,
and the SNR improved from an initial value of about 1 to 4.6.
The crescent at the top of the cyst was an artifact arising from
scattered luminescence focused by the meniscus. EM gain
(576) was enabled to acquire the image shown in Fig. 6(c)
that had significantly reduced background levels compared
with Figs. 6(a) and 6(b). The SNR for this image was im-
proved to around 28 (199/7) by virtue of background suppres-
sion and signal strength enhancement delivered by the camera
with EM gain enabled.

Our results support the conclusion that substantial im-
provements in SNR can be achieved in TGL mode without a
shutter when EM gain and frame averaging are employed.
Increased optical throughput to detector, decreased instrument
complexity, and finer control of the gate-delay interval (to
maximize detection efficiency) are key benefits arising from
the elimination of the shutter.

4 Conclusion

The solid-state instrument described here implemented a short
gate-delay to capture target luminescence at maximal inten-
sity. Good image quality was achieved after a single excita-
tion cycle of $800 \mu\text{s}$ when camera EM gain was enabled.
While the excitation and exposure portion of a TGL cycle are
essentially complete after 4 ms, the acquisition process must
be extended to 40 ms to allow for the frame readout time.
This interval is still faster than the time taken for a motorized
stage to ramp up to speed, move to a new location, and sta-
bilize.

275 An important feature of TGL techniques is the reduction in
276 image complexity that facilitates the use of computer recog-
277 nition systems to process images for the identification of tar-
278 get organisms based on their morphology. We intend to inves-
279 tigate these techniques for the automated detection of
280 methicillin-resistant *Staphylococcus Aureus* (MRSA) in spu-
281 tum samples.

282 For TGL microscopy, the introduction of inexpensive
283 solid-state LED excitation sources was an exciting develop-
284 ment, and the recent availability of EM cameras was equally
285 significant. The cost of implementing TGL microscopy has
286 plummeted while image resolution, SNR, and acquisition
287 rates have improved greatly. With solid-state instrumentation,
288 we believe that TGL microscopy has finally come of age.

289 Acknowledgments

290 We wish to thank the Australian Research Council (ARC) and
291 Olympus Australia for their generous assistance and support
292 under the ARC Linkage Program (LP0775196).

293 References

- 294** 1. A. A. Thayer and M. Sernitz, "Fluorescence techniques in cell biol-
295 ogy," in *Proc. of a conference held at the Battelle Seattle Research*
296 *Center, Seattle, Washington, March 27-31, 1972*, Springer-Verlag,
297 Berlin, 420 pp (1973).
- 298** 2. G. Bottiroli, "Time resolved fluorescence microscopy: a new tool in
299 chromatin study," *Basic Appl. Histochem.* **25**(4), 297-302 (1981).
- 300** 3. G. Marriott, R. M. Clegg, D. J. Arndt-Jovin, and T. M. Jovin. "Time
301 resolved imaging microscopy. Phosphorescence and delayed fluores-
302 cence imaging," *Biophys. J.* **60**(6), 1374-1387 (1991).
- 303** 4. J. Gadella, W. J. Theodorus, T. M. Jovin, and R. M. Clegg, "Fluores-
304 cence lifetime imaging microscopy (FLIM): Spatial resolution of mi-
305 crostructures on the nanosecond time scale," *Biophys. Chem.* **48**(2),
306 221-239 (1993).
- 307** 5. M. Rulli, A. Kuusisto, J. Salo, H. Kojola, and O. Simell, "Time-
308 resolved fluorescence imaging in islet cell autoantibody quantitation,"
309 *J. Immunol. Methods* **208**, 169-179 (1997).
- 310** 6. J. Wu, G. Wang, D. Jin, J. Yuan, Y. Guan, and J. Piper, "Luminescent
311 europium nanoparticles with a wide excitation range from UV to
312 visible light for biolabeling and time-gated luminescence bioimag-
313 ing," *Chem. Commun. (Cambridge)* **3**, 365-367 (2008).
- 314** 7. R. Pal and D. Parker, "A single component ratiometric pH probe with
315 long wavelength excitation of europium emission," *Chem. Commun.*
316 *(Cambridge)* **5**, 474-476 (2007).
- 317** 8. A. Dadabhoy, S. Faulkner, and P. G. Sammes, "Long wavelength
318 sensitizers for europium(III) luminescence based on acridone deriva-
319 tives," *J. Chem. Soc., Perkin Trans. 2* **2**, 348-357 (2002).
- 320** 9. R. C. Leif, L. M. Vallarino, M. C. Becker, and S. Yang, "Increasing
321 the luminescence of lanthanide complexes," *Cytometry* **69A**(8), 767-
322 778 (2006).
- 323** 10. H. B. Beverloo, A. van Schadewijk, S. van Gelderen-Boele, and H. J.
324 Tanke, "Inorganic phosphors as new luminescent labels for immuno-
325 cytochemistry and time-resolved microscopy," *Cytometry* **11**(7),
326 784-792 (1990).
- 327** 11. B. D. Venetta, "Microscope phase fluorimeter for determining the
328 fluorescence lifetimes of fluorochromes," *Rev. Sci. Instrum.* **30**, 450-
329 457 (1959).
12. L. Seveus, M. Vaisala, S. Syrjanen, M. Sandberg, A. Kuusisto, R.
 Harju, J. Salo, I. Hemmila, H. Kojola, and E. Soini, "Time-resolved
 fluorescence imaging of europium chelate label in immunohisto-
 chemistry and *in-situ* hybridization," *Cytometry* **13**(4), 329-338
 (1992).
13. H. B. Beverloo, A. van Schadewijk, J. Bonnet, R. van der Geest, R.
 Runia, N. P. Verwoerd, J. Vrolijk, J. S. Ploem, and H. J. Tanke,
 "Preparation and microscopic visualization of multicolor luminescent
 immunophosphors," *Cytometry* **13**(6), 561-570 (1992).
14. N. P. Verwoerd, E. J. Hennink, J. Bonnet, C. R. van der Geest, and H.
 J. Tanke, "Use of ferro-electric liquid crystal shutters for time-
 resolved fluorescence microscopy," *Cytometry* **16**(2), 113-117
 (1994).
15. T. Gadella, J. Goedhart, A. van Hoek, and A. Visser, "Construction
 and applications of a frequency-domain fluorescence lifetime imag-
 ing microscope," *Prog. Biophys. Mol. Biol.* **65**(Supplement 1), 92
 (1996).
16. R. Connally, D. Veal, and J. Piper, "Flashlamp excited time-resolved
 fluorescence microscope suppresses autofluorescence in water con-
 centrates to deliver 11-fold increase in signal to noise ratio," *J.*
Biomed. Opt. **9**(4), 725-734 (2004).
17. R. J. Hennink, R. de Haas, N. P. Verwoerd, and H. J. Tanke, "Evalu-
 ation of a time-resolved fluorescence microscope using a phosphores-
 cent Pt-porphine model system," *Cytometry* **24**, 312-320 (1996).
18. A. A. Zotikov and Y. S. Polyakov, "The use of the phosphorescence
 microscope for the study of the phosphorescence of various cells,"
Microsc. Acta **79**(5), 415-418 (1977).
19. A. S. Verkman, M. Armijo, and K. Fushimi, "Construction and evalu-
 ation of a frequency-domain epifluorescence microscope for lifetime
 and anisotropy decay measurements in subcellular domains," *Bio-*
phys. Chem. **40**(1), 117-125 (1991).
20. R. de Haas, R. P. M. van Gijlswijk, E. B. van der Tol, H. J. M. A. A.
 Zijlmans, T. Bakker-Schut, J. Bonnet, N. P. Verwoerd, and H. J.
 Tanke, "Platinum porphyrins as phosphorescent label for time-
 resolved microscopy," *J. Histochem. Cytochem.* **45**(9), 1279-1292
 (1997).
21. K. Hanaoka, K. Kikuchi, S. Kobayashi, and T. Nagano, "Time-
 resolved long-lived luminescence imaging method employing lumi-
 nescent lanthanide probes with a new microscopy system," *J. Am.*
Chem. Soc. **129**(44), 13502-13509 (2007).
22. N. P. Verwoerd, E. J. Hennink, J. Bonnet, C. R. G. van der Geest, and
 H. J. Tanke, "Use of ferro-electric liquid crystal shutters for time-
 resolved fluorescence microscopy," *Cytometry* **16**, 113-117 (1994).
23. R. E. Connally, D. A. Veal, and J. Piper, "High intensity solid-state
 UV source for time-gated luminescence microscopy," *Cytometry*
69A, 1020-1027 (2006).
24. D. Jin, R. Connally, and J. Piper, "Ultrasensitive time-resolved nano-
 liter volume fluorometry based on UV LEDs and a channel photo-
 multiplier tube," *Proc. SPIE* **5699**, 237-245 (2005).
25. D. Jin, R. Connally, and J. Piper, "Long-lived visible luminescence of
 UV LEDs and impact on LED excited time-resolved fluorescence
 applications," *J. Phys. D* **39**, 461-465 (2006).
26. R. E. Connally, D. A. Veal, and J. Piper, "Time-resolved fluorescence
 microscopy using an improved europium chelate BHHST for the in-
 situ detection of *Cryptosporidium* and *Giardia*," *Microsc. Res. Tech.*
64, 312-322 (2004).
27. G. Vesey, J. S. Slade, M. Byrne, K. Shepherd, and C. R. Fricker, "A
 new method for the concentration of *Cryptosporidium* oocysts from
 water," *J. Appl. Bacteriol.* **75**(1), 82-86 (1993).